

## Article

# Bandwidth Density Analysis of Coded Free-Space Optical Interconnects

Hasan A. Aldiabat <sup>1,\*</sup>, Nedal K. Al-Ababneh <sup>2</sup> and Asma A. Alqudah <sup>1</sup>

<sup>1</sup> Department of Telecommunications Engineering, Yarmouk University, Irbid 21163, Jordan; asma.qudah@yu.edu.jo

<sup>2</sup> Department of Electrical Engineering, Jordan University of Science and Technology, Irbid 22110, Jordan; nedalk@just.edu.jo

\* Correspondence: hasan.aldiabat@yu.edu.jo; Tel.: +962-2-7211111 (ext. 4301)

**Abstract:** The performance of free-space optical interconnects (FSOIs) system is significantly influenced by noise, similar to any wireless communication system. This noise has a notable impact on both the bandwidth density and data rate of FSOIs system. To address these challenges, this study proposes the utilization of vertical-cavity-surface-emitting laser (VCSEL) arrays on the transmitter side and photodetector arrays on the receiver side for FSOIs. The study investigates the bandwidth density of the system with and without coding while maintaining a specific bit error rate. An analysis is conducted in the presence of higher-order modes in the laser beams of the FSOIs system and a fundamental Gaussian operating mode. The presence of the higher-order modes leads to degradation in the performance of the FSOIs system in terms of bandwidth density. In addition, we examine the impact of the signal-to-noise ratio (SNR) on the system's bandwidth density for each considered operating mode. The provided simulation results clearly demonstrate that coding significantly enhances the bandwidth density of the systems, with the extent of improvement being closely tied to the employed code rate and codeword length.

**Keywords:** coded optical interconnects; optical wireless communications; RS correction codes; crosstalk noise



**Citation:** Aldiabat, H.A.; Al-Ababneh, N.K.; Alqudah, A.A. Bandwidth Density Analysis of Coded Free-Space Optical Interconnects. *Electronics* **2023**, *12*, 3873. <https://doi.org/10.3390/electronics12183873>

Academic Editors: Imran Shafique Ansari, Chen Chen and Xiong Deng

Received: 4 August 2023

Revised: 2 September 2023

Accepted: 4 September 2023

Published: 13 September 2023



**Copyright:** © 2023 by the authors. Licensee MDPI, Basel, Switzerland. This article is an open access article distributed under the terms and conditions of the Creative Commons Attribution (CC BY) license (<https://creativecommons.org/licenses/by/4.0/>).

## 1. Introduction

Free-space optical interconnects (FSOIs) systems were developed to cope with recent progress in supercomputing systems, making them a highly desirable choice for various applications in the era of big data [1]. One significant advantage of FSOIs systems is the high bandwidth capacity. They provide wide bandwidth capabilities, allowing for the transmission of large volumes of data at exceptionally fast speeds. This makes the systems particularly suitable for applications that demand rapid and efficient data communication, such as high-performance computing, cloud computing, and data centers. By leveraging FSOIs, organizations can effectively handle the increasing data requirements of the modern digital landscape [2]. Another advantage of FSOIs is the low interference susceptibility. Unlike traditional wired interconnects, FSOIs operate through free space; therefore, the potential for electromagnetic interference (EMI) and radio frequency interference (RFI) is minimized. The absence of physical cables and the utilization of optical signals mitigate the impact of electrical noise, resulting in improved signal quality and reduced transmission errors. This interference immunity is crucial in environments where reliable and high-quality data communication is essential, such as in mission-critical applications, financial transactions, and sensitive data transfers. Scalability is another key benefit of FSOIs. These interconnects offer the capability to expand the interconnect capacity by incorporating additional optical channels. This scalability is particularly valuable in scenarios where the demand for data transfer capacity can rapidly increase, such as in large-scale data centers or communication networks. By leveraging FSOIs, organizations can seamlessly

accommodate growing data requirements and adapt to evolving business needs without significant infrastructure overhauls [3,4]. FSOIs are also known for their lower power consumption compared to traditional wired interconnects. By utilizing optical signals through free space, FSOIs significantly reduce the power requirements associated with data transmission. This translates to lower energy consumption and reduced operational costs; therefore, FSOI systems can be considered to be environmentally friendly and cost-effective solutions for data-intensive applications. Furthermore, the reduced power consumption contributes to improved energy efficiency and sustainability, aligning with organizations' green initiatives and overall environmental responsibility. Flexibility and mobility are additional advantages of FSOIs. These interconnects offer unparalleled flexibility in terms of positioning and alignment. Unlike physical cables, FSOIs can be easily adjusted, re-aligned, or repositioned; this provides greater flexibility in network configurations and layouts. This adaptability is particularly valuable in scenarios where dynamic network setups are required, such as in wireless communication between mobile devices, satellite communication, or unmanned aerial vehicles (UAVs). FSOIs enable efficient and reliable communication in environments where physical connections are impractical or challenging to implement. Enhanced security is yet another benefit of FSOIs. Due to the highly directional nature of the optical beam used in FSOIs, the chances of eavesdropping or interception are significantly reduced. The narrow beam confines the transmission within a specific path, minimizing the risk of data breaches or unauthorized access. This makes FSOIs an attractive choice for secure communication in sensitive environments, including military applications, government communications, and financial institutions, where data confidentiality is of utmost importance [5,6].

Various technologies of optical interconnects—to include FSOIs, waveguides, and fibers, which can be compared across many aspects, as demonstrated in Table 1—can be assessed in terms of bandwidth density. That is identified as the time–space density product assessed at a fixed value of the operating power [7,8]. A considerably large optical capacity can be realized upon using an array of parallel spatial channels of FSOIs [9,10]. Therefore, the use of FSOI arrays has witnessed large growth in many technologies, including optical sensing, illumination, data communications, and laser printing [11–14]. However, there are some limiting factors, including noise sources, that affect the performance of FSOIs.

FSOI channels, like other wireless communication channels, are not immune to the detrimental effects of noise. Noise can degrade the performance of FSOIs systems and limit their data transmission capabilities [15]. Two primary sources of noise impact FSOI channels: channel-to-channel crosstalk and thermal noise associated with the detector amplifier. Channel-to-channel crosstalk occurs when there is an overlapping or interference of signals between adjacent channels in FSOIs systems. This phenomenon is primarily caused by light diffraction, which leads to signal leakage and interference among neighboring links. Crosstalk noise can result in a decrease in signal quality, increased bit errors, and a reduction in the achievable data rate. Managing and mitigating channel-to-channel crosstalk is crucial for ensuring reliable and high-performance FSOI communication. Thermal noise is another significant source of noise in FSOI channels and is associated with the presence of detector amplifiers. Thermal noise occurs due to the random thermal energy present in the system that leads to fluctuations in the electrical signal generated by the detector. This noise contributes to the overall noise floor of FSOI systems. Therefore, it limits the FSOIs systems' ability to discern and accurately detect low-level optical signals. The presence of thermal noise can impact the sensitivity and signal-to-noise ratio (SNR) of the FSOIs systems, affecting the achievable data rate and overall system performance. Both channel-to-channel crosstalk and thermal noise impose limitations on the data rate and capacity of FSOI interconnects. These noise sources introduce errors, decrease the reliability of the transmitted data, and may require additional resources for error correction and mitigation [16,17]. Managing and reducing these noise sources are critical considerations in the design and implementation of FSOI systems.

**Table 1.** Properties of FSOs and waveguides and fibers.

Comparison Aspect	FSOs	Waveguides and Fibers
Interference	Prone to interference from atmospheric conditions, such as fog, rain, or dust, which can degrade signal quality.	More immune to external interference due to the confinement of signals within the waveguide.
Security	Vulnerable to eavesdropping due to the nature of free-space transmission. Signals can potentially be intercepted.	More secure, as the guided signals are confined within the physical medium, making interception more challenging.
Transmission Medium	Use free space as the transmission medium, meaning they transmit optical signals through open air or vacuum.	Use guided optical signals within waveguides, such as optical fibers or integrated optical waveguides.
Atmospheric Condition	Highly dependent on the atmospheric conditions, weather, and potential obstacles in the line of sight, which can affect signal quality.	Less affected by external conditions, as the guided optical signals are contained within the waveguides.
Interconnecting Distance	Generally, more suitable for relatively short-range communication, typically up to a few kilometers.	Can support much longer distances, ranging from short distances within data centers to transcontinental communication.
Application Area	Used in scenarios where temporary or short-range high-speed communication is needed, like between chips, interconnecting buildings or data centers within close proximity.	Commonly used for backbone data center connections, long-distance telecommunications, and internet infrastructure.
Flexibility	Offer flexibility in establishing connections over short distances without the need for physical cables, making them suitable for temporary setups.	Provide more structured and permanent connections suitable for long-term setups.
Bandwidth	Can provide high bandwidth, suitable for applications with demanding data transfer rates.	Also offer high bandwidth capabilities, making them suitable for high-speed data transmission.

By understanding and effectively managing noise sources, FSOI systems can achieve higher data rates, improved signal quality, and increased reliability, enabling their successful deployment in a wide range of applications that require fast and reliable wireless optical communication. Therefore, we investigate in this article the performance of FSOI systems employing the fundamental and higher-order transverse modes of operation with and without coding. In particular, the effect of using Reed–Solomon codes (RSCs) on improving the bandwidth density of free-space optical channels is discussed. We analyze the optimum coding gain capability for reducing the signal-to-noise (SNR) ratio required to achieve a desired bit error rate in the model operation. Section 2 presents a summary of the work related to the study of this article. In Section 3, we include both a design description for the used FSOI system model and a mathematical derivation for the normalized optical intensity of the considered modes of operation. Bandwidth density simulation results of an uncoded FSOI system are presented in Section 4. We provide in Section 5 the coding impact on the bandwidth density of the investigated modes along with numerical results. Finally, the conclusion and some ideas for future work are stated in Section 6.

## 2. Related Work

Researchers and engineers have developed various techniques to mitigate noise in FSOI channels. These include lenses, advanced coding schemes, adaptive equalization techniques, spatial diversity, and optical beamforming methods. By employing these techniques, the impact of noise can be minimized, allowing for improved data transmission rates, increased link reliability, and enhanced overall system performance. For example,

the author of [15] optimized the signal-to-crosstalk ratio in an FSOI system that utilized microlenses. The author considered two scenarios for optimizing the signal-to-crosstalk ratio of the system. One scenario was for an aligned FSOI system, and the other was for a misaligned system. The conclusion was that the optimum signal-to-crosstalk ratio can be obtained by utilizing the detector size as an optimization parameter. In addition, the authors of [18] studied the performance improvement of optical interconnects in terms of data rate and spatial density due to using Reed–Solomon (RS) codes. They highlighted the significant role that coding plays in improving the capacity and misalignment tolerance of FSOI systems. However, the study overestimated the power amount of the crosstalk noise, which led to suboptimal results. The authors of [19] examined the utilization of error correction codes (ECCs), particularly Reed–Solomon codes, along with the fill factor of the receiver array on the bandwidth density. They provided numerical results that demonstrated the significance of using ECCs and the optimum fill factor value in order to enhance the bandwidth density. It was shown that different codeword lengths at different code rate levels provide different gain factors to the system's bandwidth density. Golay code deployment as a forward error correction scheme in optical interconnect systems is considered in [20]. The researchers demonstrated the feasibility of exploiting Golay codes to substitute for erasures, such as misalignment problems, a dead optical transmitter or receiver, or dark fibers, in terms of the bit error rate. In addition, the authors' investigation demonstrated that the use of forward error correction leads to decreasing the amount of optical power consumption in optical communication systems, which, in turn, decreases the requirements of launched power through the system. In [21], the authors discussed the effects of coding and fill factor on the bandwidth density of misaligned FSOI systems under the operation of the fundamental and higher-order transversal modes. The provided simulation and numerical results demonstrated that a significant improvement in the misalignment tolerance and the bandwidth density is achieved upon coding and optimizing the fill factor. The results demonstrated that there is an optimum code rate and an optimum fill factor value for each investigated codeword length. In addition, the authors showed that as the length of the codeword grew, the lateral misalignment tolerance increased. In [22], the authors exploited space–time block codes in FSOI systems to enhance their immunity against noise and misalignment. In particular, the authors expanded the application of space–time coding to a  $4 \times 4$  optical channel that employs on–off keying and utilizes real intensity-based signals. The purpose of designing these codes is to improve the system's performance by leveraging the optical crosstalk that occurs in a setup consisting of multiple laser sources and photodetectors. The encoding of data is achieved through the utilization of space–time codes that are derived from orthogonal designs. The encoded data are divided into four different streams, which are transmitted at the same time using four different transmitters operating at the same wavelength. Upon reception, the signal received by the optical receiver is a composite of all transmitted signals, accompanied by the presence of noise. Decision metrics are computed by utilizing the received signals and optical channel gains. By employing maximum likelihood decoding techniques, these metrics facilitate the separation and decoding of individual signals that are sent by various transmitters. The utilization of the modified codes, based on orthogonal designs, enables straightforward maximum likelihood decoding by employing the minimum Euclidean distance as a criterion. The authors' results showed that the considered FSOI model is capable of achieving a low bit error rate on the order of  $10^{-6}$  even when there is significant misalignment between the model components. The authors of [23] utilized extended Alamouti space–time coding in conjunction with card-to-card optical links. They provided experimental results that emphasized the ability of such coding scheme in decreasing the crosstalk in the optical system and enhancing the system sensitivity. In addition, their experimental results showed that space–time coding can expand the optical interconnection range by 48%. The authors of [24] used Manchester coding along with a differential phase shift keying modulation scheme to improve the performance of free-space optical communication systems. They found that using Manchester coding reduces the error

rate and enhances the reliability of the system. These advantages were a direct result of the synchronization capabilities of the Manchester coding scheme. In [25], the authors introduced a novel two-fold turbo coding scheme to improve the performance of optical communication systems. They showed that the coding scheme significantly enhances the performance of the system in terms of the bit error rate and SNR as compared to the typical turbo coding scheme. The authors provided analytic and simulation results to support their study. The authors of [26] provided a reconfigurable beam-forming scheme to solve the problems of nonline-of-sight free-space optical communications. They used a synchronized array of optical transmitters to spatially reshape the wave fronts of the incident light beams over diffusing surfaces. This process of reshaping the wave fronts enhances the amount of diffused light intensity reaching the array of optical receivers. The authors provided experimental results that demonstrate the feasibility of wave-front shaping for overcoming the nonline-of-sight limitation in free-space optical communications.

### 3. System Model

In this section, we provide a design description of the FSOI system and a definition of the bandwidth density (BD) in terms of data rate and channel spacing. The data rate depends mainly on both the optical power received by the intended receiver and the optical crosstalk noise; hence, clear mathematical definitions of both of them are provided.

The FSOI system is composed of two arrays—one as a transmitter and the other as a receiver—with a given interconnect distance of  $D$  between the arrays; see Figure 1a. The transmitter array contains nine identical transmitters of vertical-cavity-surface-emitting lasers (VCSELs) arranged as demonstrated in Figure 1b. Likewise, the receiver array contains nine identical photodetectors (PDs) arranged as shown in Figure 1c. The design parameters  $X$ ,  $Y$ , and  $\Delta$  marked on the figures represent the VCSEL's and photodetector's diameters and the channel spacing, respectively.

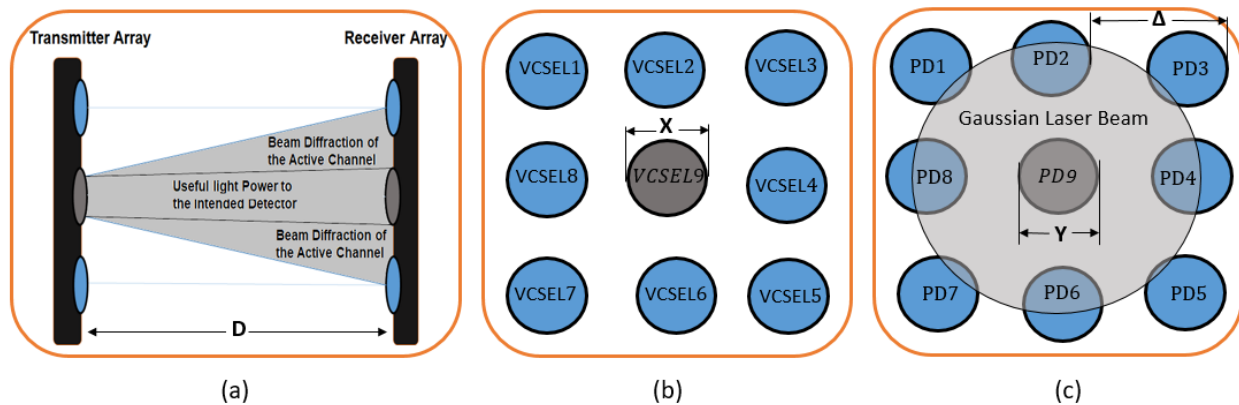


**Figure 1.** (a) Cross-sectional view of the FSOI system model and two-dimensional schematic representations of (b) nine-VCSEL array and (c) nine-photodetector array.

In fact, the exact number of channels, the distance between the source and detector arrays, and the other parameters of the FSOI system model depend on the application for which the system would be deployed. For example, in this study, we particularly used nine channels within a rectangular array shape to demonstrate the ability of using the rotational symmetry of the photodetector distribution to simplify the mathematical calculations of the crosstalk noise. From Figure 1c, it is clear that the crosstalk noise received by photodetectors 1, 3, 5, and 7 is the same, and the crosstalk noise received by photodetectors 2, 4, 6, and 8 is also the same. In addition, it should be mentioned that we used rectangular source and detector arrays—not other possibly used shapes such as hexagonal or circular shapes—for many reasons. These include that rectangular arrays are simple and easy to fabricate, align, and scale to any size. Moreover, when it comes to processing the data received by

each photodetector in the array, many signal processing and optimization techniques are naturally aligned with rectangular arrays [27–29].

The proposed FSOI system does not utilize lenses in its design. Actually, using or not using lenses completely depends on the application and the FSOI system design parameters. For example, if we try to employ the system on small printed circuit boards, such as the ones used in smart phones, where the distance between the source and the detector arrays is in the range of millimeters, the laser beam diffraction could be negligible, and using lenses in such cases would be just a waste of resources. However, if the distance between the source and the detector arrays is large, like the one mentioned in [30] where the distance between the arrays is in the range of 3 m, lenses might be used to mitigate the effect of optical interference.

The BD of an FSOI channel is defined as the ratio of the data rate ( $R$ ) and channel spacing squared, which is written as [19]

$$BD = \frac{R}{\Delta^2}. \quad (1)$$

The relationship between the BD and the used SNR as well as the FSOI model parameters can be seen from the definition of  $R$ , which is given by [19]

$$R = \frac{(P_t \times P_s - \text{SNR} \times P_t \times N)^2}{(\text{SNR} \times \text{NEP})^2}, \quad (2)$$

where  $P_t$  represents the channel's transmitted power,  $P_s$  is the optical power received by the intended receiver,  $N$  is the crosstalk noise, and NEP is the noise equivalent power that characterizes the amplifier thermal noise.

From (1) and (2), the BD of an FSOI channel can be determined by calculating  $P_s$  and  $N$  for designated  $P_t$ , NEP, SNR, and  $\Delta$  values. For example, the amount of  $P_s$  received by PD9 shown in Figure 1c from VCSEL9 shown in Figure 1b is computed by integrating the two-dimensional normalized optical intensity ( $I$ ) at the surface of photodetector 9, which is placed at a distance  $D$  from the transmitter. Assuming that the operating mode is the transverse electromagnetic  $mn$  mode ( $\text{TEM}_{mn}$ ), where  $m$  is an integer that represents the radial mode order and  $n$  is another integer that represents the angular mode order, then  $P_s$  can be formulated as

$$P_{s,mn} = \iint_{PD9} I_{mn}(r, \theta, D) r dr d\theta = \int_0^{2\pi} \int_0^{\Delta/2} I_{mn}(r, \theta, D) r dr d\theta. \quad (3)$$

As in [31], the optical intensity ( $I$ ) of an operating mode  $\text{TEM}_{mn}$  at a plane located at  $Z = D$  from a transmitter can be written as

$$I_{mn}(r, \theta, D) = \frac{4m!}{\pi \times W_D^2 \times (m+n)! \times (\delta_{0n} + 1)} \times \left(\frac{\sqrt{2}r}{W_D}\right)^{2n} \times \left(L_m^n\left(\frac{2r^2}{W_D^2}\right)\right)^2 \times \exp\left(\frac{-2r^2}{W_D^2}\right) \times \cos^2(n\theta), \quad (4)$$

where  $W_D$  is the spot size of the laser beam at the PD array located at a distance  $D$  from the VCSEL array and is given by [31]

$$W_D = W_i \sqrt{\left(\frac{2\pi \times \lambda \times D}{A^2}\right)^2 + 1},$$

where  $W_i$  is the beam waist at the transmitting laser, which is equal to  $X/(\sqrt{2}\pi)$ , and  $\lambda$  is the wavelength of operation. The

$$\delta_{0n} = \begin{cases} 1, & n = 1 \\ 0, & \text{otherwise} \end{cases}$$

and  $L_m^n(\alpha)$  is the Laguerre polynomial of order  $(m, n)$  and is defined as [32]

$$L_m^n(\alpha) = \frac{\alpha^{-n}}{m!} \times \exp(\alpha) \times \frac{d^m}{d\alpha^m} (\alpha^{m+n} \times \exp(-\alpha)),$$

Herein, we consider a laser beam with four modes of operation, which are the TEM<sub>00</sub>, TEM<sub>01</sub>, TEM<sub>10</sub>, and TEM<sub>20</sub> modes. In addition, we assume that the coupling among the laser modes is negligible. The normalized optical intensity of each mode, respectively, can be written as

$$I_{00} = \frac{2}{\pi \times W_D^2} \times \exp\left(\frac{-2r^2}{W_D^2}\right) \times \left(L_0^0\left(\frac{2r^2}{W_D^2}\right)\right)^2, \tag{5}$$

$$I_{01} = \frac{8r^2}{\pi \times W_D^4} \times \exp\left(\frac{-2r^2}{W_D^2}\right) \times \cos(\theta) \times \left(L_0^1\left(\frac{2r^2}{W_D^2}\right)\right)^2, \tag{6}$$

$$I_{10} = \frac{2}{\pi \times W_D^2} \times \exp\left(\frac{-2r^2}{W_D^2}\right) \times \left(L_1^0\left(\frac{2r^2}{W_D^2}\right)\right)^2, \tag{7}$$

and

$$I_{20} = \frac{2}{\pi \times W_D^2} \times \exp\left(\frac{-2r^2}{W_D^2}\right) \times \left(L_2^0\left(\frac{2r^2}{W_D^2}\right)\right)^2, \tag{8}$$

where  $L_0^0(\alpha) = 1$ ,  $L_0^1(\alpha) = 1$ ,  $L_1^0(\alpha) = 1 - \alpha$ , and  $L_2^0(\alpha) = 1 - 2\alpha + (1/2)\alpha^2$ .

Upon substituting the optical intensities found in (5)–(8) into (3), we can find the  $P_s$  received by the intended photodetector, which is in this case PD9, due to each mode separately.

The crosstalk noise ( $N$ ) shown in Figure 1c can be evaluated by finding the amount of incident power on the photodetectors that are not intended to receive the power from VCSEL9. The noise of the fundamental mode TEM<sub>00</sub> is defined as

$$\begin{aligned} N_{00} &= \frac{2}{\pi \times W_D^2} \sum_{j=1}^8 \iint_{PD_j} \exp\left(\frac{-2r^2}{W_D^2}\right) r dr d\theta \\ &= \frac{4 \times 2}{\pi \times W_D^2} \int_0^{2\pi} \int_0^{\Delta/2} \exp\left(\frac{-2r_1^2}{W_D^2}\right) r dr d\theta \\ &\quad + \frac{4 \times 2}{\pi \times W_D^2} \int_0^{2\pi} \int_0^{\Delta/2} \exp\left(\frac{-2r_2^2}{W_D^2}\right) r dr d\theta. \end{aligned} \tag{9}$$

where  $r_1^2 = (r \cos(\theta) - \Delta)^2 + (r \sin(\theta))^2$  and  $r_2^2 = (r \cos(\theta) - \Delta)^2 + (r \sin(\theta) + \Delta)^2$ . It should be mentioned that in (9), we exploited the photodetectors' distribution symmetry and the rotational symmetry of the laser beam. Therefore, the noise amount received by photodetectors 1, 3, 5, and 7 is the same, and the amount received by photodetectors 2, 4, 6, and 8 is the same as well.

For the other considered modes of operation—TEM<sub>01</sub>, TEM<sub>10</sub>, and TEM<sub>20</sub>, respectively—the noises of each are defined as follows

$$\begin{aligned} N_{01} &= \frac{8}{\pi \times W_D^4} \sum_{j=1}^8 \iint_{PD_j} r^2 \times \exp\left(\frac{-2r^2}{W_D^2}\right) \times \cos(\theta) r dr d\theta \\ &= \frac{4 \times 8}{\pi \times W_D^4} \int_0^{2\pi} \int_0^{\Delta/2} r_1^2 \times \exp\left(\frac{-2r_1^2}{W_D^2}\right) \times \cos(\theta) r dr d\theta \\ &\quad + \frac{4 \times 8}{\pi \times W_D^4} \int_0^{2\pi} \int_0^{\Delta/2} r_2^2 \times \exp\left(\frac{-2r_2^2}{W_D^2}\right) \times \cos(\theta) r dr d\theta, \end{aligned} \quad (10)$$

$$\begin{aligned} N_{10} &= \frac{2}{\pi \times W_D^2} \sum_{j=1}^8 \iint_{PD_j} \exp\left(\frac{-2r^2}{W_D^2}\right) \times \left(1 - \frac{2r^2}{W_D^2}\right)^2 r dr d\theta \\ &= \frac{4 \times 2}{\pi \times W_D^2} \int_0^{2\pi} \int_0^{\Delta/2} \exp\left(\frac{-2r_1^2}{W_D^2}\right) \times \left(1 - \frac{2r_1^2}{W_D^2}\right)^2 r dr d\theta \\ &\quad + \frac{4 \times 2}{\pi \times W_D^2} \int_0^{2\pi} \int_0^{\Delta/2} \exp\left(\frac{-2r_2^2}{W_D^2}\right) \times \left(1 - \frac{2r_2^2}{W_D^2}\right)^2 r dr d\theta, \end{aligned} \quad (11)$$

and

$$\begin{aligned} N_{20} &= \frac{2}{\pi \times W_D^2} \sum_{j=1}^8 \iint_{PD_j} \exp\left(\frac{-2r^2}{W_D^2}\right) \times \left(1 - 4\frac{2r^2}{W_D^2} + 0.5\left(\frac{2r^2}{W_D^2}\right)^2\right)^2 r dr d\theta \\ &= \frac{4 \times 2}{\pi \times W_D^2} \int_0^{2\pi} \int_0^{\Delta/2} \exp\left(\frac{-2r_1^2}{W_D^2}\right) \times \left(1 - 4\frac{2r_1^2}{W_D^2} + 0.5\left(\frac{2r_1^2}{W_D^2}\right)^2\right)^2 r dr d\theta \\ &\quad + \frac{4 \times 2}{\pi \times W_D^2} \int_0^{2\pi} \int_0^{\Delta/2} \exp\left(\frac{-2r_2^2}{W_D^2}\right) \times \left(1 - 4\frac{2r_2^2}{W_D^2} + 0.5\left(\frac{2r_2^2}{W_D^2}\right)^2\right)^2 r dr d\theta, \end{aligned} \quad (12)$$

Upon calculating the values of  $P_s$  and  $N$  for each of the aforementioned modes, the BD can be determined for any given SNR,  $P_t$ , and NEP, as demonstrated numerically in the following section.

#### 4. Bandwidth Density of Uncoded FSOI System

Herein, we demonstrate how the FSOI systems' design parameters affect the bandwidth density (BD) without the use of coding. Particularly, we illustrate the channel spacing ( $\Delta$ ) and signal-to-noise ratio (SNR) effects on the bandwidth density under the operation of the fundamental-order Gaussian mode of the laser beam and the investigated higher-order modes. For all simulation results provided in this manuscript, we set the design parameters to be as follows: transmitted power per channel ( $P_t$ ) of 50  $\mu$ W, operating wavelength ( $\lambda$ ) of 0.85  $\mu$ m, interconnect distance ( $D$ ) of 20 mm, VCSEL diameter ( $X$ ) of 0.03 mm, noise equivalent power (NEP) of 0.1 nW/ $\sqrt{\text{Hz}}$ , and PD diameter ( $Y$ ) of 0.8 of the channel spacing ( $\Delta$ ) distance. It should be mentioned that the used design parameter values represent typical approximate values for the operation of VCSELs and photodetectors at room temperature [1,5,33].

In Figure 2, we illustrate the effect of  $\Delta$  on the BD using the TEM<sub>00</sub>, TEM<sub>01</sub>, TEM<sub>10</sub>, and TEM<sub>20</sub> operating modes. These results were generated using a SNR of 10 dB. It is clear that each considered operating mode of the laser beam has an optimal channel spacing ( $\Delta_{opt}$ ) value. For the fundamental-order Gaussian mode (TEM<sub>00</sub>), the  $\Delta_{opt}$  that achieves the maximum bandwidth density is 0.4 mm. At relatively small values of  $\Delta$  ( $<2.6 \times 10^{-4}$  m),

the BD of the system is quite small in comparison to the optimal BD; hence, it is not depicted on Figure 2. For TEM<sub>01</sub>, TEM<sub>10</sub>, and TEM<sub>20</sub> modes, the  $\Delta_{opt}$ s are 0.54 mm, 0.66 mm, and 0.9 mm, respectively.

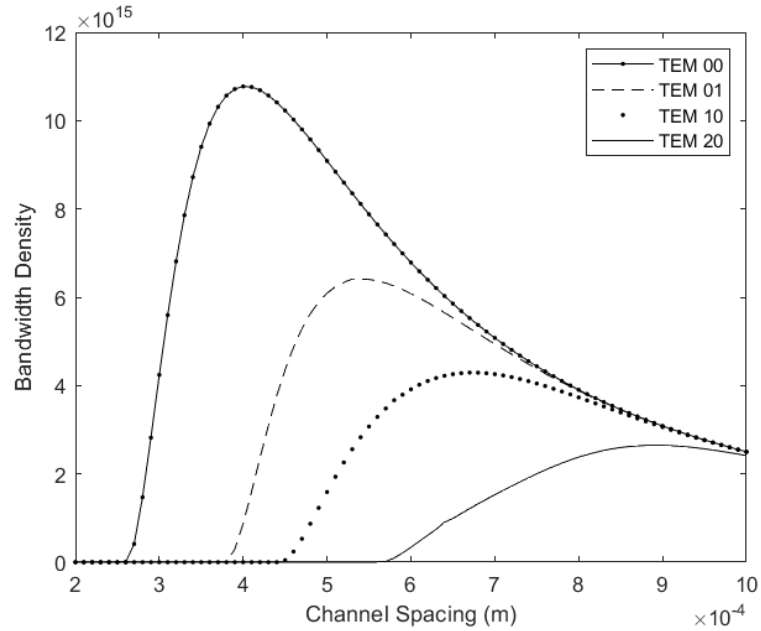


Figure 2. Bandwidth density of the FSOI system.

Figure 3 shows a relationship between the BD and the SNR of the studied operating modes. Herein, we consider the  $\Delta$  of each mode of the FSOI system equal to its  $\Delta_{opt}$ s shown in Figure 2. One can clearly see from the results that the BD is strongly correlated to the utilized SNR, and the relationship can be estimated as  $BD \propto 1/SNR^2$ . This suggests the employment of coding in order to enhance the BD, as demonstrated in the following section.

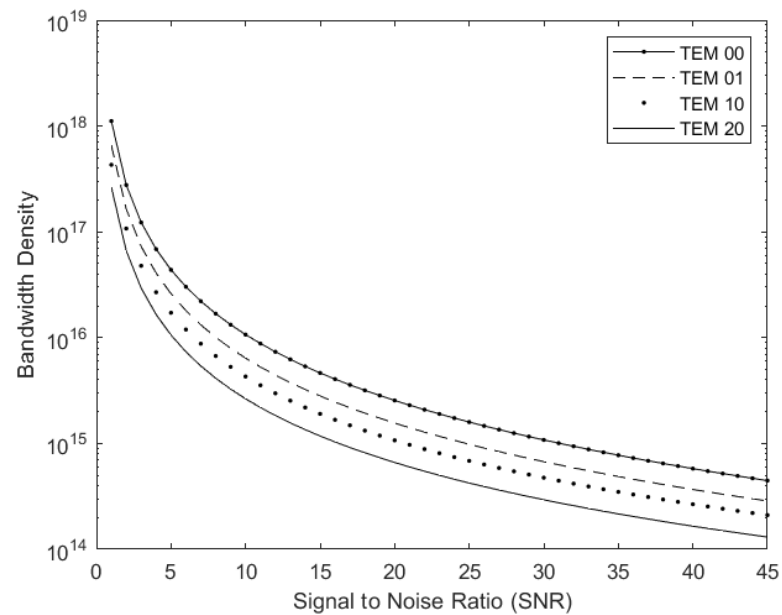


Figure 3. Bandwidth density versus SNR in dB.

### 5. Bandwidth Density of Coded FSOI System

Error correction codes (ECCs) can be exploited in the FSOI systems’ design to introduce correction capability and enhance the operational BD. The system correction capability reduces the SNR level needed to obtain a desired bit error rate (*BER*). Therefore, this capability of the system can be perceived in terms of SNR coding gain (*G*), which is defined as the ratio of the SNR needed without coding over the one with coding ( $G = SNR_{uncoded} / SNR_{coded}$ ) for a given *BER* [18]. A variety of ECCs are available in the literature [2,20,34], and they are characterized by the *G*, where a high *G* means good error correction capability. In this paper, we exploit Reed–Solomon (RS) ECCs of different codeword lengths to illustrate the effect of coding on the FSOI system BD. The characteristics of this type of codes are widely investigated in the literature, and the codes are exploited in many storage and communication systems [35–37]. To demonstrate the consequence of RS codes on the BD of optical interconnects, we analyze their *G* for a range of code rates, as shown in Figure 4. The figure is generated based on the following formulations of *BER* [19,38].

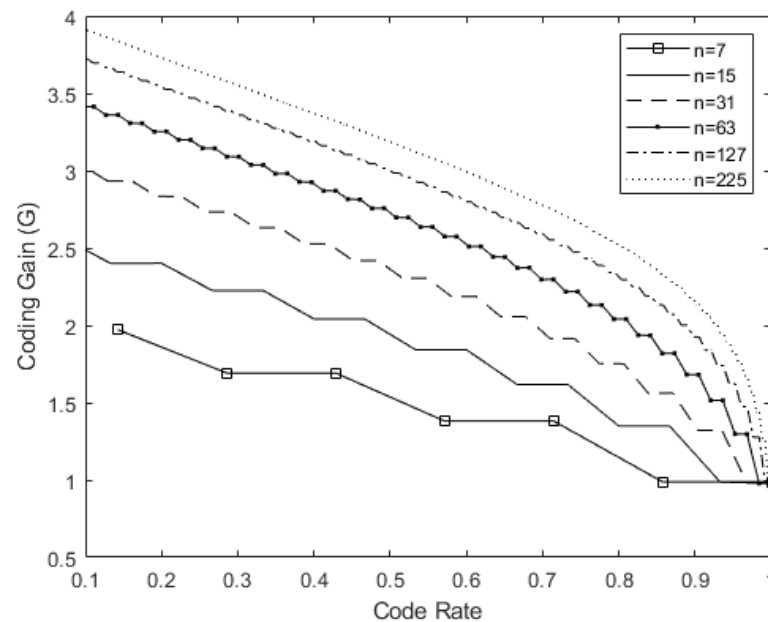


Figure 4. Coding gain for six distinct codeword lengths (*n*) of RS-ECC at *BER* of  $10^{-12}$ .

$$BER_{uncoded} = \frac{1}{2} \left( 1 - \operatorname{erf} \left( \frac{1}{2} \sqrt{\frac{SNR_{uncoded}}{2}} \right) \right), \tag{13}$$

$$BER_{coded} = \frac{1}{2} \left( 1 - \operatorname{erf} \left( \frac{1}{2} \sqrt{\frac{SNR_{coded}}{2}} \right) \right), \tag{14}$$

and

$$BER_s = 1 - (1 - BER_{coded})^m, \tag{15}$$

where erf in (13) and (14) represents the Gauss error function, which is given by  $\operatorname{erf}(\alpha) = \frac{2}{\sqrt{\pi}} \int_0^\alpha \exp(-v^2) dv$ .

The idea of using the *G* curves to enhance the bandwidth density can be explained as follows: If we consider a codeword length (*n*) of 127 with a code rate of 0.64, then from Figure 4, we find out that *G* is 2.7. This indicates that the signal-to-noise ratio level utilized to obtain the findings of Figure 2 can be decreased from 10 to 3.7 ( $10 \div 2.7$ ) while keeping

the  $BER$  without any change. This reduction in the level of  $SNR$  is converted into a gain in the  $BD$  ( $G_{BD}$ ), which is given by [18]

$$G_{BD} = \frac{BD_e - BD_u}{BD_u}, \quad (16)$$

where  $BD_u$  and  $BD_e$ , respectively, are the uncoded  $BD$  and the effective  $BD$  (defined as the code rate multiplied by the coded bandwidth density ( $BD_c$ )). Figure 5 demonstrates the relationship between the  $G_{BD}$  and the code rate for six different codeword lengths—7, 15, 31, 63, 127, and 255—with  $SNR_{uncoded} = 10$  dB. It is clear that the coding rate is a crucial parameter that influences the  $G_{BD}$  upon coding and should be considered carefully in the design process. Low values of code rates provide a lot of redundancy, which in turn reduces the  $G_{BD}$ . On the other hand, high values of code rates introduce inadequate error correction capability, which also limits the  $G_{BD}$ . Therefore, a trade-off between high and low values of code rates should be considered. From Figure 5, each codeword length has an optimum code rate that needs to be selected in the design of optical interconnects to achieve the optimal  $G_{BD}$ . For example, when the codeword length is 31, the optimum code rate is about 0.6, and it is about 0.68 for a codeword length of 255. One more observation from Figures 4 and 5 is that as the length of the codewords increases, the coding power improves in terms of both optimum coding gain and  $G_{BD}$ .

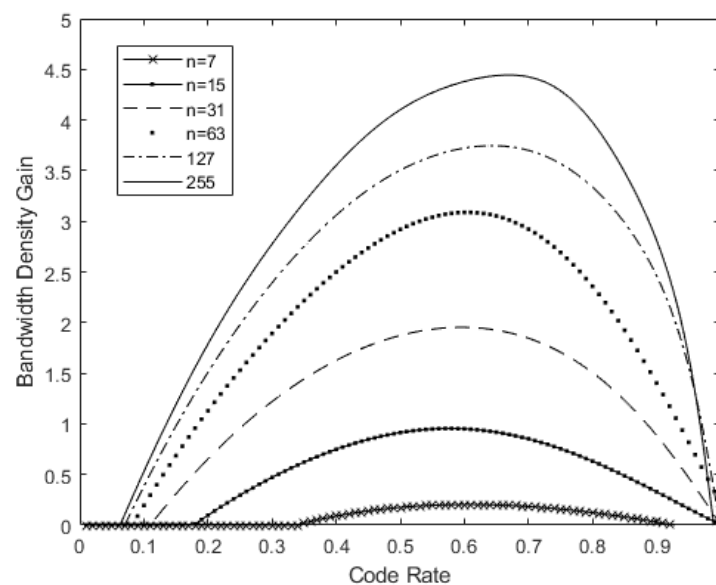


**Figure 5.** Bandwidth density gain for six distinct codeword lengths ( $n$ ) of RS-ECC.

In the following, we consider the dependence of the  $BD$  of the fundamental-order Gaussian mode ( $TEM_{00}$ ) of the laser beam and the other investigated higher-order transverse modes on coding. Figure 6a demonstrates the  $BD$  of the  $TEM_{00}$  mode before and after using Reed–Solomon error correction codes (RS-ECCs). The codes are used at the optimum data rates of each codeword length that is demonstrated in Figure 5. From the figure, the optimum data rates of the codeword lengths 15, 31, 63, 127, and 255 are 0.59, 0.61, 0.62, 0.65, and 0.68, respectively. At the optimum data rates, RS-ECCs achieve the best possible improvement to the  $BD$  of optical interconnects. This improvement is due to the ability of coding to reduce the  $SNR$  required to obtain a given  $BER$ , and in turn, this increases the  $BD$  of interconnects. In the simulation results presented in this paper, we used  $SNR_{uncoded} = 10$  dB, which means the  $SNR_{uncoded}$  for codeword lengths of 15, 31, 63, 127, and 255 at their designated optimum data rates would be 5.4, 4.6, 4.0, 3.6, and 3.5 dB, respectively. Figure 6b–d demonstrate the effect of using RS-ECC on the higher-order transverse modes  $TEM_{01}$ ,  $TEM_{10}$ , and  $TEM_{20}$ , respectively. It is clear from the results that increasing the length of the codewords leads to a direct increase in the  $BD$ . In addition,

the optimal channel spacing that achieves the maximum BD is the same with and without coding for all investigated modes.

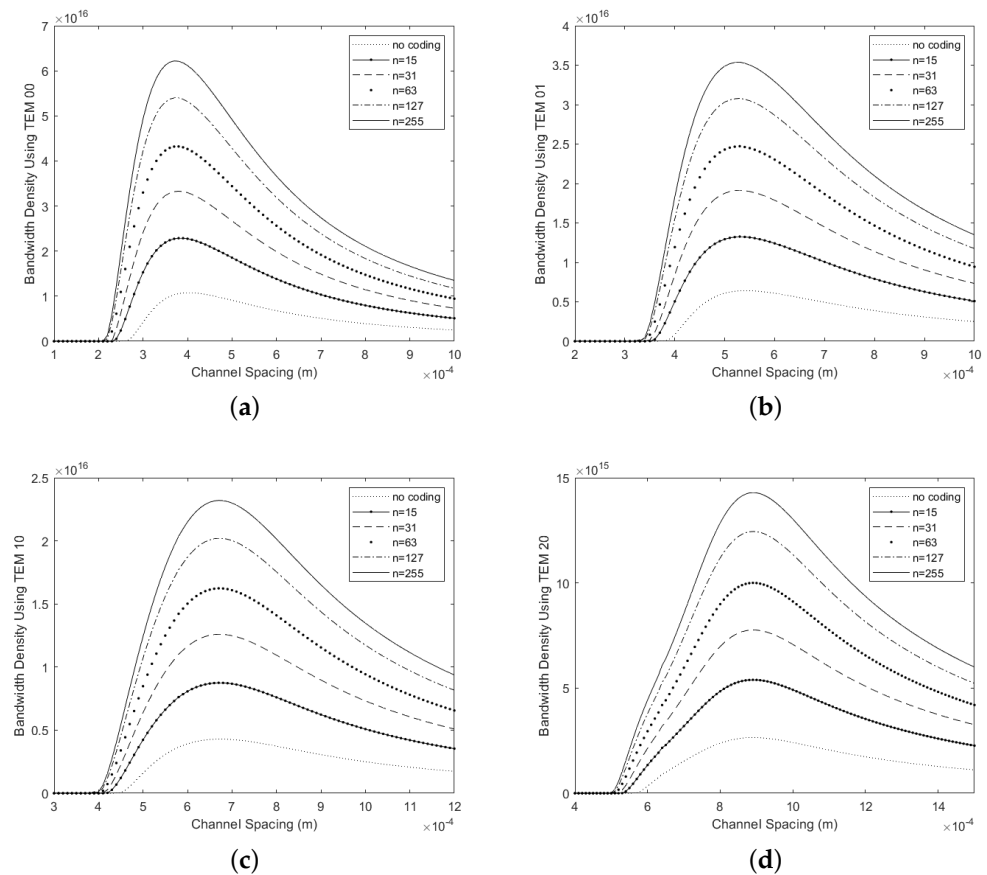


**Figure 6.** BD versus channel spacing without and with using RS-ECC of codeword lengths ( $n$ ) 15, 31, 63, 127, and 255 for (a) TEM<sub>00</sub>, (b) TEM<sub>01</sub>, (c) TEM<sub>10</sub>, and (d) TEM<sub>20</sub> modes.

## 6. Conclusions

In this paper, we have analyzed the bandwidth density (BD) of an FSOI system employing arrays of laser sources and detectors with and without coding. Moreover, the effect of reducing the SNR for a given bit error rate via coding to improve the BD has been demonstrated. Particularly, we have studied the impact of utilizing Reed–Solomon error correction codes to improve the BD of the FSOI system model under the operation of the fundamental- and higher-order modes of the laser beam. The BD performance has been analyzed in the presence of both crosstalk and thermal noise sources. The provided numerical results have shown that the BD was significantly improved due to coding at the optimum code rate of each different investigated codeword length. The ideas presented in this paper can be expanded to comprise microlenses in the FSOI system’s design in order to mitigate the crosstalk noise. Moreover, other kinds of coding schemes can be investigated.

**Author Contributions:** Conceptualization, H.A.A. and N.K.A.-A.; Formal analysis, H.A.A., N.K.A.-A. and A.A.A.; Investigation, H.A.A., N.K.A.-A. and A.A.A.; Methodology, H.A.A., N.K.A.-A. and A.A.A.; Project administration, H.A.A. and N.K.A.-A.; Software, H.A.A., N.K.A.-A. and A.A.A.; Supervision, N.K.A.-A.; Validation, H.A.A., N.K.A.-A. and A.A.A.; Writing—original draft, H.A.A.; Writing—review and editing, H.A.A., N.K.A.-A. and A.A.A. All authors have read and agreed to the published version of the manuscript.

**Funding:** This research received no external funding.

**Conflicts of Interest:** The authors declare no conflict of interest.

## References

1. Liu, A.; Wolf, P.; Lott, J.A.; Bimberg, D. Vertical-cavity surface-emitting lasers for data communication and sensing. *Photonics Res.* **2019**, *7*, 121–136. [[CrossRef](#)]
2. Wang, K.; Lim, C.; Wong, E.; Alameh, K.; Kandeepan, S.; Skafidas, E. High-speed reconfigurable free-space optical interconnects with carrierless-amplitude-phase modulation and space-time-block code. *J. Light. Technol.* **2018**, *37*, 627–633. [[CrossRef](#)]
3. Zhao, X.; Zhu, L.; Fu, S.; Liu, C.; Tang, M.; Liu, D. Dual-Band Accelerating Beams Enabled Full Duplex Free-Space Optical Interconnection. *IEEE J. Sel. Top. Quantum Electron.* **2021**, *27*, 3700107. [[CrossRef](#)]
4. Seurin, J.F.; Zhou, D.; Xu, G.; Miglo, A.; Li, D.; Chen, T.; Guo, B.; Ghosh, C. High-efficiency VCSEL arrays for illumination and sensing in consumer applications. In Proceedings of the Vertical-Cavity Surface-Emitting Lasers XX, San Francisco, CA, USA, 13–18 February 2016; Volume 9766. [[CrossRef](#)]
5. Ciftcioglu, B.; Berman, R.; Zhang, J.; Darling, Z.; Wang, S.; Hu, J.; Xue, J.; Garg, A.; Jain, M.; Savidis, L.; et al. A 3-D integrated intrachip free-space optical interconnect for many-core chips. *IEEE Photonics Technol. Lett.* **2010**, *23*, 164–166. [[CrossRef](#)]
6. Esener, S.; March, P. Present and future needs of free-space optical interconnects. In *Parallel and Distributed Processing: 15 IPDPS 2000 Workshops Cancun, Mexico*; Proceedings 14; Springer: Berlin/Heidelberg, Germany, 2000; pp. 1104–1109.
7. Hu, W.; Li, X.; Yang, J.; Kong, D. Crosstalk analysis of aligned and misaligned free-space optical interconnect systems. *J. Opt. Soc. Am. A* **2010**, *27*, 200–205. [[CrossRef](#)]
8. Al-Ababneh, N. On capacity improvement of optical free space chip-to-chip interconnects. *Electr. Eng.* **2007**, *89*, 451–456. [[CrossRef](#)]
9. Châteauneuf, M.; Kirk, A.G.; Plant, D.V.; Yamamoto, T.; Ahearn, J.D. 512-channel vertical-cavity surface-emitting laser-based free-space optical link. *Appl. Opt.* **2002**, *41*, 5552–5561. [[CrossRef](#)]
10. Kirk, A.G.; Plant, D.V.; Ayliffe, M.H.; Châteauneuf, M.; Lacroix, F. Design rules for highly parallel free-space optical interconnects. *IEEE J. Sel. Top. Quantum Electron.* **2003**, *9*, 531–547. [[CrossRef](#)]
11. Grabherr, M. New applications boost VCSEL quantities: Recent developments at Philips. In Proceedings of the Vertical-Cavity Surface-Emitting Lasers XIX, San Francisco, CA, USA, 7–12 February 2015; Volume 9381. [[CrossRef](#)]
12. Larsson, A. Advances in VCSELs for communication and sensing. *IEEE J. Sel. Top. Quantum Electron.* **2011**, *17*, 1552–1567. [[CrossRef](#)]
13. Tatum, J. VCSEL proliferation. In Proceedings of the Vertical-Cavity Surface-Emitting Lasers XI, San Jose, CA, USA, 20–25 January 2007; Volume 6484. [[CrossRef](#)]
14. Mukoyama, N.; Otoma, H.; Sakurai, J.; Ueki, N.; Nakayama, H. VCSEL array-based light exposure system for laser printing. In Proceedings of the Vertical-Cavity Surface-Emitting Lasers XII, San Jose, CA, USA, 19–24 January 2008; Volume 6908. [[CrossRef](#)]
15. Al-Ababneh, N. Crosstalk in misaligned free space optical interconnects: Modelling and simulation. *Int. J. Electr. Comput. Eng. IJECE* **2019**, *9*, 1620–1629. [[CrossRef](#)]
16. Tsai, F.C.F.; Petrovic, N.S.; Rakic, A.D. Comparison of stray-light and diffraction-caused crosstalk in free-space optical interconnects. In *Photonics: Design, Technology, and Packaging*; SPIE: Bellingham, WA, USA, 2004; Volume 5277, pp. 320–327.
17. Al-Ababneh, N.; Al Jumah, A. Analytical models for channel crosstalk in short-range free space optical interconnects. *Opt. Eng.* **2012**, *51*, 115401. [[CrossRef](#)]
18. Neifeld, M.A.; Kostuk, R.K. Error correction for free-space optical interconnects: Space-time resource optimization. *Appl. Opt.* **1998**, *37*, 296–307. [[CrossRef](#)] [[PubMed](#)]
19. Al-Ababneh, N.; Tawalbeh, S. Optimizing bandwidth density in free space optical interconnects under the use of error correcting codes. *Opt. Quantum Electron.* **2014**, *46*, 271–282. [[CrossRef](#)]
20. Faucher, J.; Venditti, M.B.; Plant, D.V. Application of parallel forward-error correction in two-dimensional optical-data links. *J. Light. Technol.* **2003**, *21*, 466–475. [[CrossRef](#)]
21. Aldiabat, H.; Al-ababneh, N. Bandwidth density optimization of misaligned optical interconnects. *Int. J. Electr. Comput. Eng. IJECE* **2022**, *12*, 1626–1635. [[CrossRef](#)]
22. Chinta, S.V.; Kurzweg, T.P.; Pfeil, D.S.; Dandekar, K.R.  $4 \times 4$  space-time codes for free-space optical interconnects. In Proceedings of the Photonics Packaging, Integration, and Interconnects IX, SPIE, San Jose, CA, USA, 24–29 January 2009; Volume 7221, pp. 297–304. [[CrossRef](#)]
23. Wang, K.; Nirmalathas, A.; Lim, C.; Alameh, K.; Skafidas, E. Space-time-coded high-speed reconfigurable card-to-card free-space optical interconnects. *J. Opt. Commun. Netw.* **2017**, *9*, A189–A197. [[CrossRef](#)]
24. Padhy, J.B.; Patnaik, B. Multiplexed free-space optical system design using Manchester coding. *Optik* **2018**, *174*, 266–273. [[CrossRef](#)]
25. Chen, J.; Huang, D.; Yuan, X. Analysis of optical wireless communication system based on a novel turbo code. *Opt. Eng.* **2006**, *45*, 125006. [[CrossRef](#)]
26. Cao, Z.; Zhang, X.; Osnabrugge, G.; Li, J.; Vellekoop, I.M.; Koonen, A.M. Reconfigurable beam system for non-line-of-sight free-space optical communication. *Light Sci. Appl.* **2019**, *8*, 69. [[CrossRef](#)]
27. Zeng, H.; Zhang, C.S.; Zhang, S. Optimal quadratic element on rectangular grids for H 1 problems. *BIT Numer. Math.* **2021**, *61*, 665–689. [[CrossRef](#)]

28. Miao, Z.; Zhang, J. Optimizing finite-difference scheme in multidirections on rectangular grids based on the minimum norm. *Geophysics* **2022**, *87*, F41–F54. [[CrossRef](#)]
29. Mohammed, J.R. Rectangular grid antennas with various boundary square-rings array. *Prog. Electromagn. Res. Lett.* **2021**, *96*, 27–36. [[CrossRef](#)]
30. Fernandes, M.A.; Monteiro, P.P.; Guiomar, F.P. Free-Space Terabit Optical Interconnects. *J. Light. Technol.* **2022**, *40*, 1519–1526. [[CrossRef](#)]
31. Wang, R.; Rakić, A.D.; Majewski, M.L. Analysis of lensless free-space optical interconnects based on multi-transverse mode vertical-cavity-surface-emitting lasers. *Opt. Commun.* **1999**, *167*, 261–271. [[CrossRef](#)]
32. Bonneux, N.; Kuijlaars, A.B.J. Exceptional Laguerre Polynomials. *Stud. Appl. Math.* **2018**, *141*, 547–595. [[CrossRef](#)]
33. Long, M.; Gao, A.; Wang, P.; Xia, H.; Ott, C.; Pan, C.; Liu, E.; Chen, X.; Lu, W.; Nilges, T.; et al. Room temperature high-detectivity mid-infrared photodetectors based on black arsenic phosphorus. *Sci. Adv.* **2017**, *3*, e1700589. [[CrossRef](#)]
34. Koila, S.; G.D., G.S.; Kulkarni, M.; Sripati, U. FPGA implementation of a BCH Codec for free space optical communication system. In Proceedings of the 2014 International Conference on Advances in Computing, Communications and Informatics (ICACCI), IEEE, Delhi, India, 24–27 September 2014; pp. 1822–1826. [[CrossRef](#)]
35. Costello, D.J.; Lin, S. *Error Control Coding: Fundamentals and Applications*; Prentice Hall: Hoboken, NJ, USA, 2014. [[CrossRef](#)]
36. Wang, J.; Zhang, G.; Hu, W. An efficient error control scheme for chip-to-chip optical interconnects. In Proceedings of the IEEE International Symposium on Circuits and Systems, New Orleans, LA, USA, 27–30 May 2007; pp. 3712–3715. [[CrossRef](#)]
37. Konyar, M.Z.; Öztürk, S. Reed Solomon coding-based medical image data hiding method against salt and pepper noise. *Symmetry* **2020**, *12*, 899. [[CrossRef](#)]
38. Aldiabat, H.; Alhubaishi, A. Performance analysis of dual-branch selection combining technique over the generalized Alpha-Mu fading channels. *Indones. J. Electr. Eng. Comput. Sci. IJEECS* **2021**, *22*, 1024–1031. [[CrossRef](#)]

**Disclaimer/Publisher’s Note:** The statements, opinions and data contained in all publications are solely those of the individual author(s) and contributor(s) and not of MDPI and/or the editor(s). MDPI and/or the editor(s) disclaim responsibility for any injury to people or property resulting from any ideas, methods, instructions or products referred to in the content.